

Bi₂Sr₂CaCu₂O₈ intrinsic Josephson junction stacks with improved cooling: Coherent emission above 1 THz

M. Ji,^{1,2} J. Yuan,² B. Gross,³ F. Rudau,³ D. Y. An,^{1,2} M. Y. Li,^{1,2} X. J. Zhou,^{1,2} Y. Huang,¹ H. C. Sun,¹ Q. Zhu,¹ J. Li,¹ N. Kinev,⁴ T. Hatano,² V. P. Koshelets,⁴ D. Koelle,³ R. Kleiner,³ W. W. Xu,¹ B. B. Jin,¹ H. B. Wang,^{1,2,a)} and P. H. Wu¹

¹Research Institute of Superconductor Electronics, Nanjing University, Nanjing 210093, China

²National Institute for Materials Science, Tsukuba 3050047, Japan

³Physikalisches Institut and Center for Collective Quantum Phenomena in LISA+, Universität Tübingen, D-72076 Tübingen, Germany

⁴Kotel'nikov Institute of Radio Engineering and Electronics, 125009 Moscow, Russia

(Received 18 July 2014; accepted 16 September 2014; published online 25 September 2014)

We report on Bi₂Sr₂CaCu₂O₈ (BSCCO) intrinsic Josephson junction stacks with improved cooling, allowing for a remarkable increase in emission frequency compared to the previous designs. We started with a BSCCO stack embedded between two gold layers. When mounted in the standard way to a single substrate, the stack emits in the range of 0.43–0.82 THz. We then glued a second, thermally anchored substrate onto the sample surface. The maximum voltage of this better cooled and dimension-unchanged sample was increased and, accordingly, both the emission frequencies and the tunable frequency range were significantly increased up to 1.05 THz and to 0.71 THz, respectively. This double sided cooling may also be useful for other “hot” devices, e.g., quantum cascade lasers. © 2014 AIP Publishing LLC. [<http://dx.doi.org/10.1063/1.4896684>]

Terahertz (THz) technology has attracted increasing attention for decades due to its potential applications in detection and imaging, for instance, in the context of high-altitude telecommunications, public security, food quality control, and environmental monitoring.^{1,2} In terms of compact solid state devices, THz quantum cascade lasers (QCLs) are good oscillators for frequencies above 2 THz,³ while intrinsic Josephson junction (IJJ) stacks show good performance at sub-THz frequencies, typically between 0.4 and 0.8 THz.^{4,5} In order to bridge the THz gap, the semiconducting QCLs have to move downwards with their operation frequencies and the superconducting IJJs emitters have to go to the opposite direction. Very interestingly, in both cases, the main challenge is to overcome the self-heating caused by the applied dc power.

The supercurrent across a Josephson junction biased at a voltage V_0 oscillates at a frequency $f_e = 2eV_0/h$, where e is the elementary charge and h is the Planck constant. When N junctions in an array oscillate coherently, the emission power can be scaled up to N^2P_0 , where P_0 is the emission power from a single junction, typically in the order of pW to nW. To reach a useful power level, N should be as large as possible. In the high transition temperature (T_c), superconductor Bi₂Sr₂CaCu₂O₈ (BSCCO) IJJs are naturally formed by the layered crystal structure, with a density of 670 junctions/ μm .⁶ Stacks of 1000 IJJs can easily be fabricated and by geometry the stack can serve as a cavity to make all junctions in the stack oscillate coherently. In 2007, coherent THz emission up to 0.85 THz was successfully detected in 1 μm thick and large-sized BSCCO IJJs mesas,⁷ and later on was observed^{8–25} and analyzed^{26–42} for different bias current regimes and various structures. Several applications have been realized for THz absorption¹⁵ or reflection imaging⁴³ and for computed

tomography imaging.⁴⁴ However, with a few exceptions¹⁸ in most experiments, the emission frequencies were well below 1 THz. The main obstacle to get higher frequencies is self-heating, which limits the maximum voltage V_{max} across the stack.⁸ This self-heating is getting more severe with more junctions in the stack. Self-heating is a double-edged sword for the THz emission. A heat-induced hot-spot, which formed at “high-bias”,^{9,11,16,20,23,25,34,37,40–42,45} can be helpful to narrow the emission line and to tune the frequency range.^{9,14,16,46} However, it raises the sample temperature in both the “hot” and the “cold” parts of the stack, reduces V_{max} , and consequently limits the highest Josephson frequency based on the relation $f_{max} = 2eV_{max}/hN$.

The strong self-heating of IJJ stacks is not only caused by the relatively high input dc power but also by the poor c -axis thermal conductivity of BSCCO. In the conventional mesa structure, a stack of IJJs stands on a thick BSCCO base crystal, through which the heat diffuses from the mesa to the substrate. Further, the base crystal seems to decrease the maximum emission power. It has been found that a gold-BSCCO-gold (GBG) structure, i.e., a bare IJJ stack contacted by two gold layers can emit THz emission with a directly detected power as high as $\sim 25 \mu\text{W}$, considerably larger than that of the conventional mesas.^{19,24,47}

In the present work, we started from fabricating a GBG structure, and then put another substrate on the top of the as-prepared sample, using polyimide as glue and thermal anchor. At given bias current I and bath temperature T_b , the total voltage V across the stack as well as the terahertz emission frequencies were significantly increased compared to the GBG stack mounted to only one substrate. The highest emission frequencies reached 1.05 THz, and the highest power was doubled compared to the pristine stack.

BSCCO single crystals with $T_c \sim 88 \text{ K}$ were grown using a floating zone technique.¹³ The fabrication technique of the

^{a)}Electronic mail: hbwang1000@gmail.com

GBG structure is similar to that of the double-sided structure reported earlier.¹³ Here, we describe the main steps involved in the process. Sketches of the pristine stack are shown in Figs. 1(a) and 1(c) and sketches of the stack covered by two substrates are shown in Figs. 1(b) and 1(d).

To form the pristine stack, a BSCCO single crystal was glued on a silicon substrate with polyimide. Then, a 200 nm thick gold film was deposited onto the crystal immediately after cleaving. As the third step, a $300 \times 50 \mu\text{m}^2$ rectangular mesa was fabricated using photolithography. The thickness of mesa was $1.5 \mu\text{m}$ involving ~ 1000 IJJs. The sample was then glued to a MgO substrate using polyimide, indicated in Fig. 1(c) as MgO-1 and Polyimide-1, respectively. Next, the base crystal was cleaved away by removing the silicon substrate, leaving the mesa standing alone surrounded by Polyimide-1. The fresh surface was immediately covered with a 100 nm thick gold layer. Photoresist was patterned in a rectangular, $230 \times 150 \mu\text{m}^2$ wide area over the cleaved mesa using photolithography, and then the whole sample was etched down to the bottom gold layer by ion milling, resulting in a $1.5 \mu\text{m}$ thick mesa with lateral dimensions of $230 \times 50 \mu\text{m}^2$ and contacted by the top and bottom gold layers.

The as-prepared GBG sample was mounted onto a silicon lens with a diameter of 6 mm and set in a helium flow cryostat with a THz transparent polyethylene window for emission detection experiments. A THz interferometer with a Si bolometer was used to measure the spectrum of the THz emission with a resolution of about 15 GHz. Note that the top gold electrode can reflect the radiation of the IJJ stack to the MgO substrate and then to the silicon lens.

Having characterized the GBG, we carefully glued another MgO substrate (MgO-2) onto the GBG sample with Polyimide-2, cf. Figs. 1(b) and 1(d). Thus, a sandwich structure (SWS) was finally realized with the BSCCO mesa embedded between two substrates. The transport and emission experiments were carried out again like for the pristine GBG.

Fig. 2(a) shows the current-voltage curves (IVCs) at $T_b = 30$ K of the GBG and the SWS. The linear contact resistance of the GBG (3.6Ω) and the nonlinear contact resistance of the SWS have been subtracted.⁴⁸ In fact, in the high-bias regime, this nonlinearity causes uncertainties and a systematic error in determining V approximately on a 5% level.

For the IVC of the GBG, shown by the blue line, weak voltage switches were observed at $I = 17$ mA and 22 mA, corresponding to the resistive states of a few junctions. At $I = 32$ mA, all junctions are switched to their normal states. By further increasing I to 60 mA and then back to zero, the outmost branch was obtained, with the typical heating-induced S shape. The highest voltage is ~ 2.05 V. The red line in Fig. 2(a) indicates the IVC of the SWS. The difference between the IVCs of the two structures is remarkable. In the voltage state, although both of the high-bias regimes have a similar profile with a negative differential resistance on the outmost branches, the highest voltage of the SWS reaches ~ 2.50 V, being 25% larger than that of the GBG. Despite these changes, there is good evidence that hot-spot formation occurs both in the GBG and the SWS, although the top MgO substrate prevented direct hot-spot imaging. It has been shown that in a plot of dc input power, P_{dc} vs. I hot-spot formation shows up as a kink followed by an almost linearly increasing part, see Fig. 9 in Ref. 40. Fig. 3 shows the corresponding plot for both structures. The kink and the linear slope at high currents are clearly visible. For the SWS, the kink occurs at a slightly lower bias current compared to the GBG and, for a given I in the high-bias regime, P_{dc} is higher for the SWS than for the GBG. This seems to be the main difference between the two structures.

We also calculated IVCs of the GBG and the SWS by numerically solving the heat diffusion equation with the 3D finite-element simulation software COMSOL. The simulation follows the procedure of Ref. 40, modeling the geometry of the present sample structures as good as possible, however, with some simplifications. MgO is a very good thermal

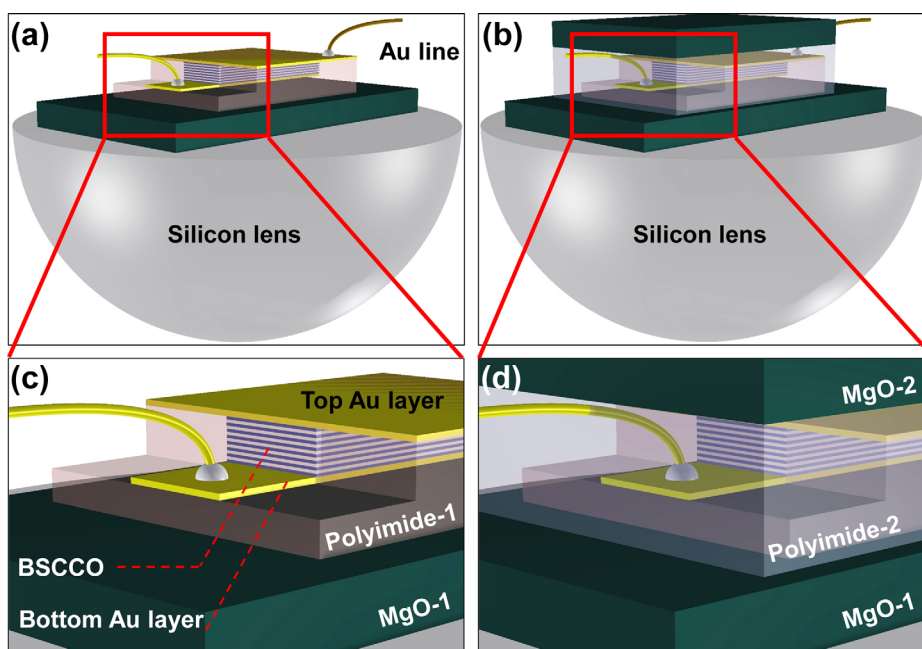


FIG. 1. Schematic views of (a) a GBG and (b) a SWS structure mounted on the silicon lens. (c) and (d) Close-ups of the IJJ stacks.

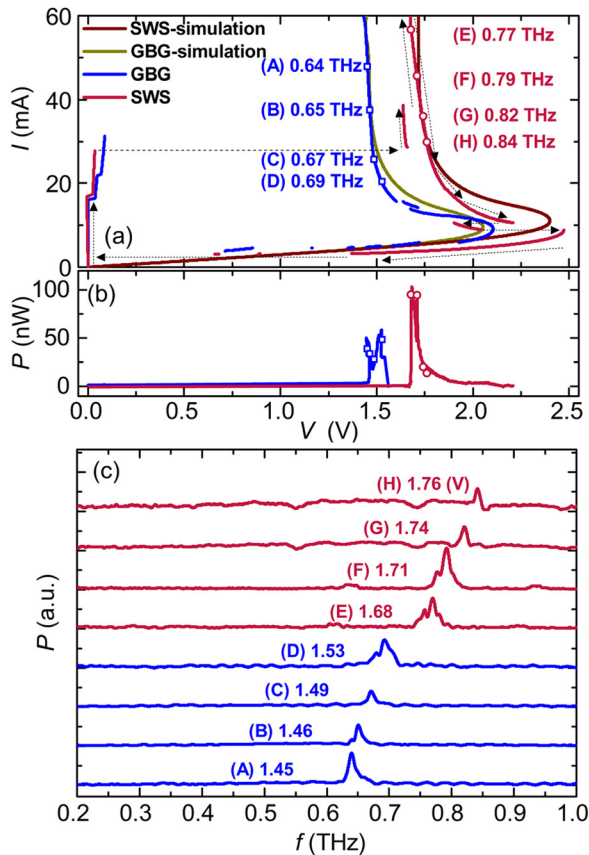


FIG. 2. Results of transport and THz emission experiments of the GBG (blue lines) and the SWS (red lines) at $T_b = 30$ K. (a) IVCs; contact resistances are subtracted. (b) Si-bolometer detected emission intensity vs. voltage across the stack. In (a), the dark yellow and wine lines are simulated IVCs for the GBG and the SWS, respectively. In (a), bias points (A)–(D) for the GBG and (E)–(H) for the SWS are marked, for which emission spectra are shown in (c). For these points, emission frequencies are indicated in (a) and voltages are indicated in (c). Arrows in (a) indicate direction of current sweeps.

conductor⁴⁹ and the bottom MgO substrate is in good thermal contact to the thermal bath. Thus, it is omitted in the simulations and the lower boundary of the bottom glue layer (Polyimide-1) is set as the cold source at T_b . The thickness ($7.5 \mu\text{m}$) of this glue layer has been adjusted so that the simulated IVC of the GBG structure matches the experimental one as good as possible. For the temperature dependence of the BSCCO in-plane and out-of-plane resistance and the

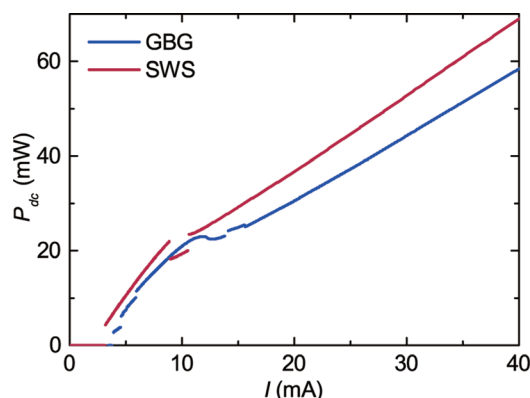


FIG. 3. dc input power P_{dc} vs. bias current I for the GBG and SWS. $T_b = 30$ K.

various electrical and thermal conductivities, we used the same dependencies as in Ref. 40. Despite these simplifications, the profile of the simulated IVC of the GBG clearly resembles the measured IVC, cf. Fig. 2(a). For the SWS, a top glue layer (Polyimide-2, $17 \mu\text{m}$ thickness) and a top MgO substrate have been added, cf. Fig. 1(d). Again, experimental and simulated IVC agree satisfactorily, cf. Fig. 2(a). Both structures show the formation of a hot-spot for high-bias currents. Representative data for the calculated temperature profiles along the length of the stack for both the GBG and the SWS at $T_b = 30$ K are shown in Ref. 50. While, at fixed I in the high-bias regime, the maximum temperature was comparable for the two structures, the hot-spot was narrower for the SWS, leading to a higher overall resistance. At low-bias also, the maximum temperature was lower for the SWS, again leading to an increased resistance.

Fig. 2(b) shows plots of the emitted radiation power P vs. V at $T_b = 30$ K. The power quoted refers to the response of the bolometer. For the GBG, THz emission was detected in the high-bias regime near $V = 1.5$ V, as shown by the blue line in Fig. 2(b). No radiation was detected at the low-bias regime. At this particular bath temperature, for the SWS (red line), the maximum emission power in the high-bias regime is almost doubled compared to that of the GBG structure. It is shifted to significantly higher voltages. In addition, the range of voltages where emission occurs is broader for the SWS. The SWS also emitted in the low-bias regime. The corresponding data are discussed further below.

For the GBG, at $V = 1.45$ V (point (A) in Fig. 2(a)), the spectrum of the emission was detected with a sharp peak at 0.64 THz (cf. curve (A) in Fig. 2(c)). Spectra for the bias points labelled (B), (C), and (D) in Fig. 2(a) are also shown in Fig. 2(c). The emission frequencies are 0.65, 0.67, and 0.69 THz for the voltages 1.46 V, 1.49 V, and 1.53 V, respectively. For the SWS, in the high-bias regime, four bias points (E), (F), (G), and (H) at voltages of, respectively, 1.68, 1.71, 1.74, and 1.76 V were selected to compare THz emission spectra with the GBG. The spectra are shown by red lines in Fig. 2(c). The emission frequencies are, respectively, 0.77, 0.79, 0.82, and 0.84 THz, much higher than those of the GBG.

The frequency ranges of detectable emission of both the GBG and the SWS with respect to T_b and V are summarized in Fig. 4. Both structures exhibit the same tendency, namely, the emission frequencies gradually increase with decreasing T_b . The GBG was found to radiate for bath temperatures below 65 K, while the emission from the SWS can be detected over a broader temperature range from 20 to 80 K, indicating that the possible operation temperature can be in the liquid nitrogen temperature range. At fixed T_b , e.g., at 20 K, the emission frequencies of the SWS ranged from 0.76 to 1.05 THz covering a considerably larger range than the GBG (0.62–0.82 THz). For the entire temperature regime, the SWS exhibits an emission frequency range (0.34–1.05 THz) which is much broader than the GBG one (0.43–0.82 THz). Note that for the SWS emission above 50 K was observed at “low bias”. Also the highest emission frequency of 1.05 THz—the corresponding spectrum is shown as an inset in Fig. 4(a)—was observed in the low-bias regime of the SWS.

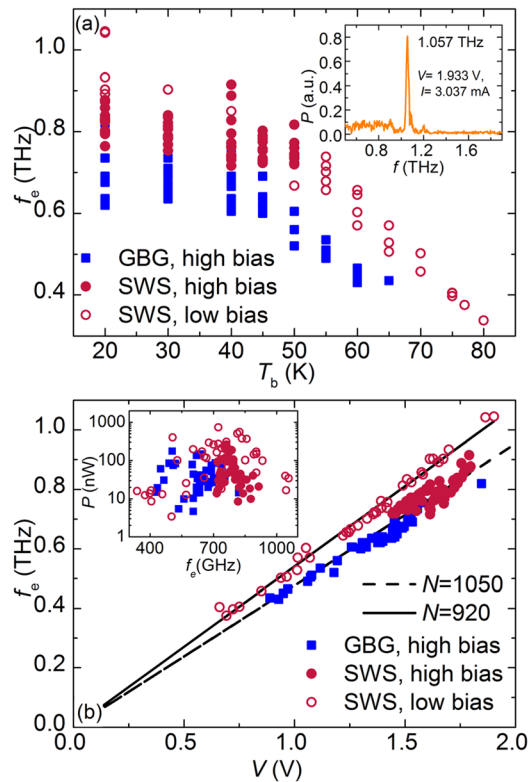


FIG. 4. Emission frequency f_e vs. (a) the bath temperature and (b) the voltage V across the mesa stacks. The lines in (b) correspond to $f_e = 2eN/hV$, with $N = 1050$ (dashed line) and $N = 920$ (solid line). The inset in (a) shows the spectrum of THz emission at $T_b = 20$ K and $I = 3.037$ mA. The inset in (b) shows the emitted power for all measured bath temperatures and bias points.

Based on the Josephson relation $f_e = 2eV_0/h$, the number N of junctions contributing to the coherent emission can be derived from $N = V/V_0 = 2eV/hf$. We plot all data of f_e vs. V in Fig. 4(b). The data of the GBG follow the dashed line, the slope of which corresponds to $2e/hN$, where N can be estimated to about 1050, not far from the estimated (from stack thickness) junction number ~ 1000 . For the SWS, the data points distribute into two parts. In the high-bias regime, the slope of f_e vs. V corresponds to $N \sim 1050$. This is comparable to the GBG, suggesting that most of the junctions have contributed to the coherent emission. In the low-bias regime, some junctions may have switched to their zero voltage states, resulting in a smaller number of emitting junctions, as indicated by the open circles in Fig. 4(b). These data follow the Josephson relation with $N \sim 920$.

Finally, in the inset of Fig. 4(b), we plot, for both the GBG and the SWS, the emission power, as detected by the bolometer, as a function of f_e for all values of T_b and I . For completeness, we have also included data points which were taken far away from the emission maxima of P vs. I . Despite the scatter, one observes that for the GBG values of P in excess of, say, 50 nW occur at frequencies between 0.45 and 0.75 THz. By contrast, the SWS shows strong emission at frequencies between 0.7 and 0.8 THz in the high-bias regime and between 0.5 and 0.9 THz at low bias. For emission frequencies above 1 THz, P is suppressed but still clearly detectable.

In summary, we have embedded an intrinsic Josephson junction stack between two gold electrodes and sandwiched

this structure between two MgO substrates, resulting in improved cooling compared to the pristine gold-BSCCO-gold structure mounted to only one substrate. For a fixed current and bath temperature, we observed a substantial increase of the total voltage across the stack and of the emission frequency. The highest emission frequency was near 1.05 THz at a bath temperature of 20 K, and the tunable frequency range was up to 0.71 THz with a single device. The method of using two substrates may also be useful for other “hot” THz devices like quantum cascade lasers.

We gratefully acknowledge financial support by the National Natural Science Foundation of China (Grant Nos. 11234006 and 61371035), the National Basic Research Program of China (No. 2011CBA00107), the CAEP THz Science and Technology Foundation (Grants Nos. 201202 and 201206), the Deutsche Forschungsgemeinschaft (Project No. KL930/12-1), and the Grants-in-Aid for scientific research from JSPS, and RFBR Grant Nos. 13-02-00493-a and 14-02-91335.

¹B. Ferguson and X. C. Zhang, *Nat. Mater.* **1**, 26 (2002).

²M. Tonouchi, *Nat. Photonics* **1**, 97 (2007).

³B. S. Williams, *Nat. Photonics* **1**, 517 (2007).

⁴U. Welp, K. Kadowaki, and R. Kleiner, *Nat. Photonics* **7**, 702 (2013).

⁵I. Kawayama, C. Zhang, H. B. Wang, and M. Tonouchi, *Supercond. Sci. Technol.* **26**, 093002 (2013).

⁶R. Kleiner, F. Steinmeyer, G. Kunkel, and P. Müller, *Phys. Rev. Lett.* **68**, 2394 (1992).

⁷L. Ozyuzer, A. E. Koshelev, C. Kurter, N. Gopalsami, Q. Li, M. Tachiki, K. Kadowaki, T. Yamamoto, H. Minami, H. Yamaguchi, T. Tachiki, K. E. Gray, W.-K. Kwok, and U. Welp, *Science* **318**, 1291 (2007).

⁸C. Kurter, K. E. Gray, J. F. Zasadzinski, L. Ozyuzer, A. E. Koshelev, Q. Li, T. Yamamoto, K. Kadowaki, W.-K. Kwok, M. Tachiki, and U. Welp, *IEEE Trans. Appl. Supercond.* **19**, 428 (2009).

⁹H. B. Wang, S. Guénon, B. Gross, J. Yuan, Z. G. Jiang, Y. Y. Zhong, M. Grünzweig, A. Iishi, P. H. Wu, T. Hatano, D. Koelle, and R. Kleiner, *Phys. Rev. Lett.* **105**, 057002 (2010).

¹⁰M. Tsujimoto, K. Yamaki, K. Deguchi, T. Yamamoto, T. Kashiwagi, H. Minami, M. Tachiki, and K. Kadowaki, *Phys. Rev. Lett.* **105**, 037005 (2010).

¹¹S. Guénon, M. Grünzweig, B. Gross, J. Yuan, Z. G. Jiang, Y. Y. Zhong, A. Iishi, P. H. Wu, T. Hatano, D. Koelle, H. B. Wang, and R. Kleiner, *Phys. Rev. B* **82**, 214506 (2010).

¹²T. M. Benseman, A. E. Koshelev, K. E. Gray, W.-K. Kwok, U. Welp, K. Kadowaki, M. Tachiki, and T. Yamamoto, *Phys. Rev. B* **84**, 064523 (2011).

¹³J. Yuan, M. Y. Li, J. Li, B. Gross, A. Ishii, K. Yamaura, T. Hatano, K. Hirata, E. Takayama-Muromachi, P. H. Wu, D. Koelle, R. Kleiner, and H. B. Wang, *Supercond. Sci. Technol.* **25**, 075015 (2012).

¹⁴M. Y. Li, J. Yuan, N. V. Kinev, J. Li, B. Gross, S. Guénon, A. Ishii, K. Hirata, T. Hatano, D. Koelle, R. Kleiner, V. P. Koshelets, H. B. Wang, and P. H. Wu, *Phys. Rev. B* **86**, 060505(R) (2012).

¹⁵M. Tsujimoto, H. Minami, K. Delfanzari, M. Sawamura, R. Nakayama, T. Kitamura, T. Yamamoto, T. Kashiwagi, T. Hattori, and K. Kadowaki, *J. Appl. Phys.* **111**, 123111 (2012).

¹⁶T. Kakeya, Y. Omukai, T. Yamamoto, K. Kadowaki, and M. Suzuki, *Appl. Phys. Lett.* **100**, 242603 (2012).

¹⁷M. Tsujimoto, T. Yamamoto, K. Delfanzari, R. Nakayama, T. Kitamura, M. Sawamura, T. Kashiwagi, H. Minami, M. Tachiki, K. Kadowaki, and R. A. Klemm, *Phys. Rev. Lett.* **108**, 107006 (2012).

¹⁸T. Kashiwagi, M. Tsujimoto, T. Yamamoto, H. Minami, K. Yamaki, K. Delfanzari, K. Deguchi, N. Orita, T. Koike, R. Nakayama, T. Kitamura, M. Sawamura, S. Hagino, K. Ishida, K. Ivancovic, H. Asai, M. Tachiki, R. A. Klemm, and K. Kadowaki, *Jpn. J. Appl. Phys., Part 1* **51**, 010113 (2012).

¹⁹D. Y. An, J. Yuan, N. V. Kinev, M. Y. Li, Y. Huang, M. Ji, H. Zhang, Z. L. Sun, L. Kang, B. B. Jin, J. Chen, J. Li, B. Gross, A. Ishii, K. Hirata, T. Hatano, V. P. Koshelets, D. Koelle, R. Kleiner, H. B. Wang, W. W. Xu, and P. H. Wu, *Appl. Phys. Lett.* **102**, 092601 (2013).

- ²⁰T. M. Benseman, A. E. Koshelev, W.-K. Kwok, U. Welp, K. Kadowaki, J. R. Cooper, and G. Balakrishnan, *Supercond. Sci. Technol.* **26**, 085016 (2013).
- ²¹T. M. Benseman, K. Gray, A. Koshelev, W.-K. Kwok, U. Welp, H. Minami, K. Kadowaki, and T. Yamamoto, *Appl. Phys. Lett.* **103**, 022602 (2013).
- ²²F. Turkoglu, L. Ozyuzer, H. Koseoglu, Y. Demirhan, S. Preu, S. Malzer, Y. Simsek, H. B. Wang, and P. Müller, *Physica C* **491**, 7 (2013).
- ²³T. M. Benseman, A. E. Koshelev, W.-K. Kwok, U. Welp, V. K. Vlasko-Vlasov, K. Kadowaki, H. Minami, and C. Watanabe, *J. Appl. Phys.* **113**, 133902 (2013).
- ²⁴S. Sekimoto, C. Watanabe, H. Minami, T. Yamamoto, T. Kashiwagi, R. A. Klemm, and K. Kadowaki, *Appl. Phys. Lett.* **103**, 182601 (2013).
- ²⁵H. Minami, C. Watanabe, K. Sato, S. Sekimoto, T. Yamamoto, T. Kashiwagi, R. A. Klemm, and K. Kadowaki, *Phys. Rev. B* **89**, 054503 (2014).
- ²⁶A. E. Koshelev, *Phys. Rev. B* **78**, 174509 (2008).
- ²⁷S. Z. Lin and X. Hu, *Phys. Rev. Lett.* **100**, 247006 (2008).
- ²⁸V. M. Krasnov, *Phys. Rev. Lett.* **103**, 227002 (2009).
- ²⁹M. Tachiki, S. Fukuya, and T. Koyama, *Phys. Rev. Lett.* **102**, 127002 (2009).
- ³⁰N. F. Pedersen and S. Madsen, *IEEE Trans. Appl. Supercond.* **19**, 726 (2009).
- ³¹S. Z. Lin and X. Hu, *Phys. Rev. B* **82**, 020504 (2010).
- ³²V. M. Krasnov, *Phys. Rev. B* **82**, 134524 (2010).
- ³³A. E. Koshelev, *Phys. Rev. B* **82**, 174512 (2010).
- ³⁴H. Asai, M. Tachiki, and K. Kadowaki, *Phys. Rev. B* **85**, 064521 (2012).
- ³⁵V. M. Krasnov, *Phys. Rev. B* **83**, 174517 (2011).
- ³⁶T. Koyama, H. Matsumoto, M. Machida, and Y. Ota, *Supercond. Sci. Technol.* **24**, 085007 (2011).
- ³⁷A. Yurgens, *Phys. Rev. B* **83**, 184501 (2011).
- ³⁸S. Z. Lin and X. Hu, *Phys. Rev. B* **86**, 054506 (2012).
- ³⁹Y. O. Averkov, V. M. Yakovenko, V. A. Yampol'skii, and F. Nori, *Phys. Rev. Lett.* **109**, 027005 (2012).
- ⁴⁰B. Gross, S. Guénon, J. Yuan, M. Y. Li, J. Li, A. Iishi, R. G. Mints, T. Hatano, P. H. Wu, D. Koelle, H. B. Wang, and R. Kleiner, *Phys. Rev. B* **86**, 094524 (2012).
- ⁴¹H. Asai and S. Kawabata, *Appl. Phys. Lett.* **104**, 112601 (2014).
- ⁴²A. Grib and P. Seidel, *Phys. Status Solidi B* **251**, 1040 (2014).
- ⁴³T. Kashiwagi, K. Nakade, B. Markovi, Y. Saiwai, H. Minami, T. Kitamura, C. Watanabe, K. Ishida, S. Sekimoto, K. Asanuma, T. Yasui, Y. Shibano, M. Tsujimoto, T. Yamamoto, J. Mirkovi, and K. Kadowaki, *Appl. Phys. Lett.* **104**, 022601 (2014).
- ⁴⁴T. Kashiwagi, K. Nakade, Y. Saiwai, H. Minami, T. Kitamura, C. Watanabe, K. Ishida, S. Sekimoto, K. Asanuma, T. Yasui, Y. Shibano, M. Tsujimoto, T. Yamamoto, B. Markovi, J. Mirkovi, R. A. Klemm, and K. Kadowaki, *Appl. Phys. Lett.* **104**, 082603 (2014).
- ⁴⁵H. B. Wang, S. Guénon, J. Yuan, A. Iishi, S. Arisawa, T. Hatano, T. Yamashita, D. Koelle, and R. Kleiner, *Phys. Rev. Lett.* **102**, 017006 (2009).
- ⁴⁶B. Gross, J. Yuan, D. Y. An, M. Y. Li, N. V. Kinev, X. J. Zhou, M. Ji, Y. Huang, T. Hatano, R. G. Mints, V. P. Koshelets, P. H. Wu, H. B. Wang, D. Koelle, and R. Kleiner, *Phys. Rev. B* **88**, 014524 (2013).
- ⁴⁷K. Kadowaki, M. Tsujimoto, K. Delfanzari, T. Kitamura, M. Sawamura, H. Asai, T. Yamamoto, K. Ishida, C. Watanabe, and S. Sekimoto, *Physica C* **491**, 2 (2013).
- ⁴⁸The IVC below the critical current exhibited a concave curvature due to the contact resistance. The voltage across the mesa was corrected using the form $V_{corr} = V_{raw} - 4.6I + 10I^{1.5}$, where V_{corr} and V_{raw} are in V and I in A.
- ⁴⁹G. A. Slack, *Phys. Rev.* **126**, 427 (1962).
- ⁵⁰See supplementary material at <http://dx.doi.org/10.1063/1.4896684> for the calculated temperature distribution in the GBG and the SWS.